Journal of Sound and Vibration (1997) **204**(3), 397–419

UNCOUPLED FLEXURAL VIBRATIONS OF STRAIGHT BEAMS WITH ALL POSSIBLE BOUNDARY CONDITIONS TREATED BY A TRANSFER MATRIX METHOD

K. B. Subrahmanyam and A. K. Garg

Department of Mechanical Engineering, N.B.K.R. Institute of Science and Technology, Vidyanagar 524 413, *India*

(*Received* 16 *October* 1995, *and in final form* 28 *August* 1996)

A computer code is developed to furnish the details of the frequencies, mode shapes (displacement, slope, shear force and bending moment) and generalized masses for the uncoupled flexural vibrations of straight beams with all possible boundary conditions, accounting for complicating effects such as shear deformation, rotary inertia, variable axial loading and flexibility of supports. A transfer matrix procedure has been used in developing the code. The results produced by the presently developed code are validated by comparison with exact solutions developed in this paper for certain cases, and also with the results available in the published literature. The code is shown to produce results of excellent accuracy, and it is believed that it will be useful to the designer in obtaining dependable results for fairly complex beam geometries with discontinuities in mass and stiffness distributions, support flexibilities and variable axial loads.

1. INTRODUCTION

There are several methods for the solution of beam vibration problems. In the continuum model approach, the minimum of potential energy, and the complementary energy methods [1, 2] are widely used. While the potential energy approach is known to produce accurate displacements and poor stresses, the complementary energy produces accurate stresses and poor displacements. In order to achieve accurately both the stress and the displacement fields simultaneously, one uses certain mixed variational principles, notable among which are the Reissner principle, and the Dean and Plass dynamic variational principle [3, 4]. Solution of the differential equations describing the motion of the beam is accomplished by the Galerkin method [5, 6], the finite difference method [7, 8], and by an improved finite difference method [9, 10]. However, as the beam geometry becomes more complex, and discontinuities in mass and stiffness distributions along with non-classical boundary conditions exist, the differential equations become more complex, the energy functional becomes more unwieldy, and the basic simplicity and appeal found in the methods discussed earlier while solving the classical type of problems will be completely overshadowed. In such situations, the methods developed by Holzer [11], Myklestad [12], and their extensions [13], termed under the category of transfer matrix methods, assume vital importance.

Thus, in the present paper the aim is to develop a computer code by using a transfer matrix procedure for the solution of the beam flexure problem with all possible boundary conditions, including a large number of complicating effects such as the shear deformation,

0022–460X/97/280397 + 23 $25.00/0/sv960925

rotary inertia, spring supports, discontinuities in mass and stiffness distributions, and variable axial tension or compression. It is believed that such a code will be of immense use to the designer to obtain a preliminary set of results (uncoupled frequencies, mode shapes and generalized masses) incorporating almost all non-classical effects. If necessary, further refinement can be achieved by consideration of the coupling between the flexural motion in two mutually perpendicular planes, torsional motion and extension. Such an analysis, and development of a computer code for coupled motions, is the subject matter of a proposed subsequent paper.

2. DEVELOPMENT OF TRANSFER MATRICES

The basic building blocks in the transfer matrix procedure are the field transfer matrix and the point transfer matrix. Pestel and Leckie [14] provide the general guidelines for the derivation of the transfer matrices. However, when a beam is subjected to axial loads, and if shear deformation and rotary inertia effects are to be included in the analysis, the relevant transfer matrices are not available in general, and one has to develop them as discussed in what follows.

2.1. FIELD TRANSFER MATRIX

For the case of a beam with axial tensile or compressive load, and including the effects of shear deformation and rotary inertia [3], the following equilibrium equations can be obtained (see Figure 1):

$$V = KGA(w' + \psi) \pm Pw', \qquad M = EI\psi', \qquad \psi' = M/EI. \tag{1–3}$$

Note that the upper sign is to be used for the case of axial tension and the lower sign for the case of axial compression in all the equations that follow, as shown in equation (1). Since each cross-sectional face rotates through an angle, ψ, the inertia couple is $\rho A i_y^2 \omega^2 \psi \, \mathrm{d}x$ and the inertia force is $\rho A \omega^2 w \, \mathrm{d}x$. Thus,

$$\mathrm{d}M/\mathrm{d}x = V - \mu i_y^2 \omega^2 \psi \mp Pw', \qquad \mathrm{d}V/\mathrm{d}x = -\mu\omega^2 w. \tag{4, 5}$$

Differentiating equation (1), equating the result to equation (5), replacing ψ' from equation (3) and simplifying, one has

$$w'' + KGA/(KGA \pm P)(M/EI) + \mu w\omega^2/(KGA \pm P) = 0. \tag{6a}$$

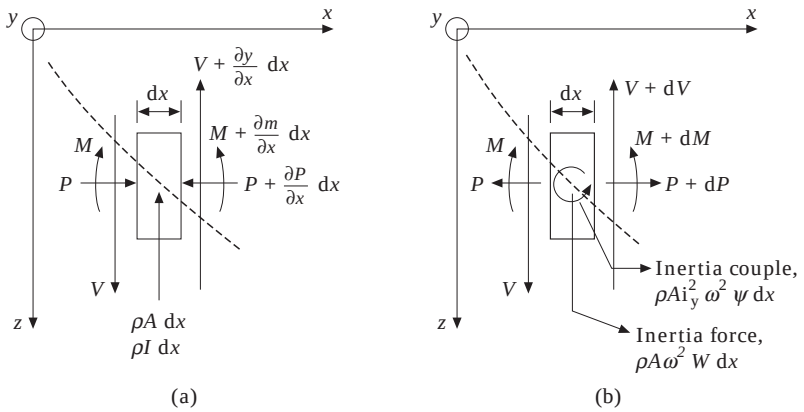

Figure 1. An element of a Timoshenko beam: (a) differential under compressive axial load; (b) differential element under tensile axial load.

Let $\zeta = KGA/(KGA \pm P)$. Then equation (6a) is given as

$$w'' + \zeta(M/EI) + \mu\omega^2 w/(KGA \pm P) = 0, \tag{6b}$$

and is rewritten as

$$M = -(EI/\zeta)[w'' + \mu\omega^2 w/(KGA \pm P)]. \tag{6c}$$

Equation (6c), when differentiated twice, yields

$$M'' = -(EI/\zeta)[w'''' + \mu\omega^2 w''/(KGA \pm P)]. \tag{7}$$

Differentiating equation (4), one has

$$M'' = V' - \mu i_y^2 \omega^2 \psi' \mp Pw'', \tag{8}$$

which can be rewritten by replacing V' from equation (5) as

$$M'' = -\mu\omega^2 w - \mu i_y^2 \omega^2 \psi' \mp Pw''. \tag{9}$$

From equations (7) and (9), one has

$$-(EI/\zeta)[w'''' + \mu\omega^2 w''/(KGA \pm P)] + \mu\omega^2 w + \mu i_y^2 \omega^2 \psi' \pm Pw'' = 0, \tag{10a}$$

which can be written as follows upon replacing $\psi' = M/EI$ from equation (6c):

$$w'''' + w''[\mu\omega^2/(KGA \pm P) \mp P\zeta/(EI) + \mu i_y^2 \omega^2/(EI)] + w[-\mu\omega^2\zeta/(EI) + \mu i_y^2 \omega^4/\{EI(KGA \pm P)\}] = 0. \tag{10b}$$

Letting

$$\sigma = \mu\omega^2 l^2/(KGA \pm P), \qquad \gamma^2 = P\zeta l^2/EI, \qquad \beta^4 = \mu\omega^2\zeta l^4/EI,$$
$$\tau = \mu i_y^2 \omega^2 l^2/(EI) \mp P\zeta l^2/(EI) = \mu i_y^2 \omega^2 l^2/(EI) \mp \gamma^2,$$

equation (10b) is rewritten as

$$w'''' + w''(\sigma + \tau)/l^2 - w(\beta^4 - \sigma\tau \mp \sigma\gamma^2)/l^4 = 0. \tag{11}$$

The solution for equation (11) may be sought as

$$w = \bar{C}\, e^{\lambda\eta}, \qquad \eta = x/l, \tag{12}$$

which, when substituted in equation (11), leads to

$$\lambda^4 + (\sigma + \tau)\lambda^2 - \{\beta^4 - \sigma\tau \mp \sigma\gamma^2\} = 0. \tag{13}$$

The roots are $\pm\lambda_1$ and $\pm i\lambda_2$ for the case of compressive loading, where

$$\lambda_{1,2} = \{[\beta^4 \mp \sigma\gamma^2 + (\sigma - \tau)^2/4]^{1/2} \mp (\sigma + \tau)^2/2\}^{1/2}. \tag{14}$$

Furthermore,

$$\lambda_2^2 - \lambda_1^2 = \sigma + \tau, \qquad \lambda_2^2\lambda_1^2 = \beta^4 \mp \sigma\gamma^2 - \sigma\tau. \tag{15}$$

Since equation (11) is of fourth order in w, one can choose a solution of the form

$$w = C_1 \cosh \lambda_1\eta + C_2 \sinh \lambda_1\eta + C_3 \cos \lambda_2\eta + C_4 \sin \lambda_2\eta, \tag{16a}$$

or, more conveniently,

$$V = A_1 \cosh \lambda_1\eta + A_2 \sinh \lambda_1\eta + A_3 \cos \lambda_2\eta + A_4 \sin \lambda_2\eta. \tag{16b}$$

Choosing equation (16b) as the solution, and noting that $w = -V'/\mu\omega^2$ as given in equation (5), one can find w. Similarly, by noting that $\psi = V/KGA - w' \mp Pw'$ as given in equation (1), one can find ψ, since V and w are already known. Finally, M is evaluated from equation (3). The resulting equations can be written in matrix notation as

$$\{Z(\eta)\} = [B(\eta)]\{a\}, \tag{17}$$

where

$$\{Z(\eta)\} = \{-w \quad \psi \quad M \quad V\}^{\mathrm{T}}, \qquad \{a\} = \{A_1 \quad A_2 \quad A \quad A_4\}^{\mathrm{T}}, \tag{18}$$

and $[B(\eta)]$ is a (4×4) matrix, the elements of which are

$$\begin{aligned}
B_{11}(\eta) &= k_1\lambda_1 \sinh \lambda_1\eta, & B_{12}(\eta) &= k_1\lambda_1 \cosh \lambda_1\eta,\\
B_{13}(\eta) &= -k_1\lambda_2 \sin \lambda_2\eta, & B_{14}(\eta) &= k_1\lambda_2 \cos \lambda_2\eta,\\
B_{21}(\eta) &= k_2P_1 \cosh \lambda_1\eta, & B_{22}(\eta) &= k_2P_1 \sinh \lambda_1\eta,\\
B_{23}(\eta) &= -k_2P_2 \cos \lambda_2\eta, & B_{24}(\eta) &= -k_2P_2 \cos \lambda_2\eta,\\
B_{31}(\eta) &= k_3P_1\lambda_1 \sinh \lambda_1\eta, & B_{32}(\eta) &= k_3P_1\lambda_1 \cosh \lambda_1\eta,\\
B_{33}(\eta) &= k_3P_2\lambda_2 \sin \lambda_2\eta, & B_{34}(\eta) &= k_3P_2\lambda_2 \cos \lambda_2\eta,\\
B_{41}(\eta) &= \cosh \lambda_1\eta, & B_{42}(\eta) &= \sinh \lambda_1\eta,\\
B_{43}(\eta) &= \cos \lambda_2\eta, & B_{44}(\eta) &= \sin \lambda_2\eta,
\end{aligned}$$

where

$$k_1 = \zeta l^3/EI\beta^4, \qquad k_2 = l^2/EI\beta^4, \qquad k_3 = l/\beta^4, \qquad P_1 = \lambda_1^2 + \sigma, \qquad P_2 = \lambda_2^2 - \sigma. \tag{19}$$

Equation (17) is next evaluated at $\eta = 0$, which can be treated as the $(i-1)$th station of the ith segment. The vector $\{a\}$ in equation (17) is found by inverting matrices. Thus,

$$\begin{Bmatrix} A_1 \\ A_2 \\ A_3 \\ A_4 \end{Bmatrix} = \begin{bmatrix} 0 & \Lambda/k_2 & 0 & \Lambda_2 \\ \Lambda_2/k_1\lambda_1 & 0 & \Lambda/k_3\lambda_1 & 0 \\ 0 & -\Lambda/k_2 & 0 & \Lambda_1 \\ \Lambda_1/k_1\lambda_2 & 0 & -\Lambda/k_3\lambda_2 & 0 \end{bmatrix} \begin{Bmatrix} -w \\ \psi \\ M \\ V \end{Bmatrix} = [B(0)]^{-1}\{Z\}_{i-1}, \tag{20}$$

where

$$\Lambda = 1/(\lambda_1^2 + \lambda_2^2), \qquad \Lambda_1 = (\lambda_1^2 + \sigma)\Lambda, \qquad \Lambda_2 = (\lambda_2^2 - \sigma)\Lambda, \qquad \Lambda_1 + \Lambda_2 = 1,$$
$$\Lambda_1\Lambda_2 = (\beta^4 \mp \sigma\gamma^2)\Lambda^2 \qquad \text{or} \qquad \beta^4 = \Lambda_1\Lambda_2/\Lambda^2 \pm \sigma\gamma. \tag{21}$$

Note that

$$\{Z\}_i = [B(\eta)]_i\{a\} = [B(\eta)]_{\eta=1}[B(0)]^{-1}\{Z\}_{i-1}. \tag{22}$$

Thus, $[B(\eta)]_{\eta=1}$ is evaluated by setting $\eta = 1$ in equation (19), the matrix multiplication prescribed in equation (22) is performed, and the resulting matrix is obtained.

There are certain advantages in treating the beam segment as massless with the mass and mass moment of inertia lumped at its end points. With such a procedure whereby the beam segment is massless, it can be demonstrated that the field transfer matrices, applicable, respectively, for the bending in the x–z plane and the y–z plane, torsion and extension, will be uncoupled from one another in terms of their respective variables of their corresponding state vectors, although the point transfer matrix will exhibit coupling among

all the variables of the state vector. In the general case of coupled bending–torsion–extensional motion for a beam with non-coincident elastic and mass axes, derivation of the transfer matrix similar to that given by the above procedure will be an uphill task [14]. With the beam treated as massless, however, the field and point transfer matrices can be formulated with relative ease, as will be demonstrated in a proposed subsequent paper. With this philosophy in mind, it is proposed to illustrate the derivation of the field transfer matrix for a massless Timoshenko beam in what follows.

2.1.1. *Field transfer matrix for tensile axial load*

One can show that for the case of a massless beam with tensile axial load, $\mu = 0$, $\sigma = 0$, $\beta = 0$, and

$$\lambda_1 = \gamma, \qquad \lambda_2 = 0, \qquad \zeta = KGA/(KGA + P), \qquad \gamma = \sqrt{(\zeta Pl^2/EI)}. \tag{23}$$

The relation (22) is written as

$$\{Z\}_i = [F]_i \{Z\}_{i-1}, \tag{24}$$

$$[F] = \begin{bmatrix} 1 & \zeta l D_1 & \zeta l^2 D_2/EI & \{\zeta l^3 D_3/EI - H_2 l/KGA\} \\ 0 & \cosh\gamma & l D_1/EI & l^2 D_2/EI \\ 0 & \zeta P l D_1 & \cosh\gamma & l D_1 \\ 0 & 0 & 0 & 1 \end{bmatrix}, \tag{25}$$

where $D_1 = (\sinh\gamma)/\gamma$, $D_2 = (\cosh\gamma - 1)/\gamma^2$ and $D_3 = (\sinh\gamma - \gamma)/\gamma^3$. Furthermore, $H_2 = 0$ if shear deformation is neglected, and $H_2 = 1$ if shear deformation is included. Note that the term l/KGA is deducted from the fourth element of the first row of the matrix, since the shear deformation effect due to axial load P was considered in the derivation of the transfer matrix, while that due to lateral load was not. Derivation of the shear deformation effect due to lateral bending which results in the presently deducted term l/KGA is straightforward [3].

2.1.2. *Reduction of the matrix for zero axial load*

When axial tensile load is absent, $P = 0$, $\gamma = 0$ leads to an indeterminate situation for several elements of the field transfer matrix. Consider, for example, the fourth element in the first row, $F_{14} = \zeta l^3(\sinh\gamma - \gamma)/(EI\gamma^3) - H_2 l/KGA$. When $\gamma = 0$, $\zeta = KGA/(KGA + P) = 1$ and $F_{14} \Rightarrow 0 \div 0$. Application of l'Hôpital's rule leads to

$$F_{14} = l^3/(6EI) - H_2 l/(KGA). \tag{26}$$

A similar procedure for all the elements leads to

$$[F] = \begin{bmatrix} 1 & l & l^2/(2EI) & \{l^3/(6EI) - H_2 l/(KGA)\} \\ 0 & 1 & l/(EI) & l^2/(2EI) \\ 0 & 0 & 1 & l \\ 0 & 0 & 0 & 1 \end{bmatrix}. \tag{27}$$

2.1.3. *Field transfer matrix for a compressive load*

For this particular case, $\mu = 0$, $\sigma = 0$, $\beta = 0$, and

$$\lambda_1 = 0, \qquad \lambda_2 = \gamma, \qquad \zeta = KGA/(KGA - P), \qquad \gamma = \sqrt{(\zeta Pl^2/EI)}. \tag{28}$$

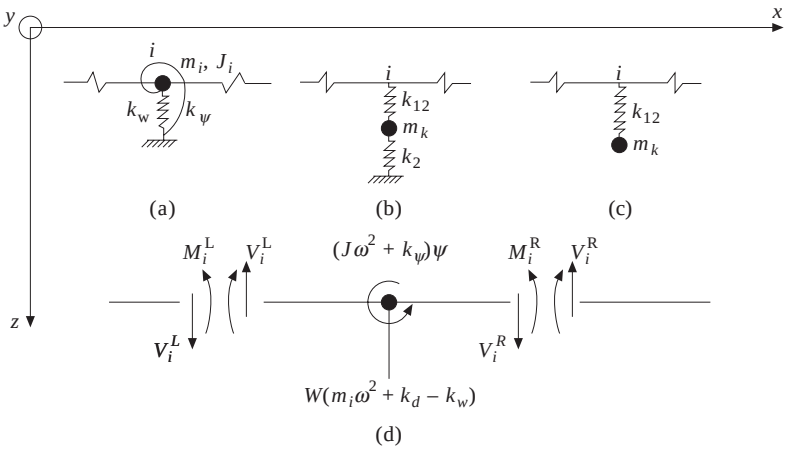

Figure 2. Details of a lumped mass, mass moment of inertia and free body diagram: (a) spring supported mass; (b), (c) spring coupled mass; (d) free body diagram.

For these parameters, the field transfer matrix is

$$[F] = \begin{bmatrix} 1 & \zeta l D_1 & \zeta l^2 D_2/EI & \{\zeta l^3 D_3/EI - H_2 l/KGA\} \\ 0 & \cos\gamma & l D_1/EI & l^2 D_2/EI \\ 0 & -\zeta P l D_1 & \cos\gamma & l D_1 \\ 0 & 0 & 0 & 1 \end{bmatrix}, \tag{29}$$

where, now, $D_1 = (\sin\gamma)/\gamma$, $D_2 = (1 - \cos\gamma)/\gamma^2$ and $D_3 = (\gamma - \sin\gamma)/\gamma^3$. For the case of zero compressive load, equation (29) reduces to that given in equation (27).

2.1.4. *Comparison of the present field transfer matrix with that available in the published literature* [15]

If the development for the general transfer matrix presented in reference [15] is compared to the present development, one can observe that there are certain differences in the way the axial force is incorporated in the equilibrium equations. In the present development, P enters into the shear equation through the total slope in a more rigorous manner [14], $V = KGA(w' + \psi) \pm Pw'$. In reference [15], P enters into M' via the bending slope, $M' = V \mp P\psi$. Consequently, the term $\zeta = KGA/(KGA \pm P)$ does not appear in the development of reference [15]. By setting $\zeta = 1$ in the present result, identical field transfer matrices as given in reference [15] can be obtained. The present development is thus believed to be more rigorous.

2.2. POINT TRANSFER MATRIX

The point transfer matrix relates the state vector $\{Z\}_i$ from the left side of the mass to the right side according to the relation

$$\{Z\}_i^R = [P]_i \{Z\}_i^L. \tag{30}$$

In order to develop the point transfer matrix, consider a mass m at a typical station supported on a linear and a rotational spring (stiffness K_w and K_ψ), having a mass moment of inertia $J = \rho A i_y^2 l$. When the beam deflects with a displacement of magnitude w and a bending slope ψ, the equilibrium relation requires that (see Figure 2)

$$\begin{Bmatrix} -w \\ \psi \\ M \\ V \end{Bmatrix} = \begin{bmatrix} 1 & 0 & 0 & 0 \\ 0 & 1 & 0 & 0 \\ 0 & (H_1 J\omega^2 + K_\psi) & 1 & 0 \\ (m\omega^2 - K_w) & 0 & 0 & 1 \end{bmatrix}_i \begin{Bmatrix} -w \\ \psi \\ M \\ V \end{Bmatrix}. \tag{31}$$

In the above matrix, H_1 is introduced for purposes of generalization. By assigning different values for H_1 and H_2 (see equations (25) and (29)), one can address the Timoshenko beam (allowing for shear deformation and rotary inertia, $H_1 = -1$ and $H_2 = 1$); the Rayleigh beam (bending with rotary inertia, $H_1 = -1$ and $H_2 = 0$); a shear beam (bending with shear deformation, $H_1 = 0$ and $H_2 = 1$), and an Euler–Bernoulli beam ($H_1 = H_2 = 0$). Although the Euler–Bernoulli beam theory disregards the effects of distributed rotary inertia, one can study the effects of a concentrated moment of inertia, as in the case of a disk mounted on a shaft. Thus, for the case of a rotating shaft, allowing for the effects of gyroscopic effects, H_1 is set equal to $+1$ or -3 for whirl in the same or the opposite direction, respectively, as rotation. Furthermore, for the particular case in which the shear deformation effects are ignored, the bending slope ψ will be equal to the total slope. Finally, if an additional spring coupled mass m_k exists at station i, the equivalent stiffness K_d is added (see Figure 2) such that

$$V_i^{\mathrm{R}} = (m\omega^2 - K_w + K_d)w + V_i^{\mathrm{L}}, \tag{32}$$

where

$$K_d = -K_{12}(K_2 - m_k\omega^2)/\{K_{12} + K_2 - m_k\omega^2\} \tag{33}$$

for case (b) of Figure 2, and K_2 is set equal to zero in equation (33) for case (c).

3. SOLUTION PROCEDURE

Consider a beam, as shown in Figure 2, discretized into n segments. Each station can have a mass and mass moment of inertia lumped, and each mass may be supported on linear and rotational springs. Each station may also have a spring supported mass as shown in Figure 2. Furthermore, the segments need not be of equal length, but each segment is assumed to have uniform flexural rigidity and shear stiffness, and the segment of the beam is assumed to be massless. The numbering of the stations starts with zero on the left end of the beam, with n being the station number of the right end.

Starting from the left of station zero, one can write the state vector for the right of station zero as

$$\{Z\}_0^{\mathrm{R}} = [P]_0\{Z\}_0^{\mathrm{L}}, \tag{34}$$

wherein the point transfer matrix at station zero, $[P]_0$, relates to the state vectors on either side of it. Considering next the segment 0–1, that has a massless field, one can write

$$\{Z\}_1^{\mathrm{L}} = [F]_1\{Z\}_0^{\mathrm{R}}, \tag{35}$$

where the field transfer matrix for segment 1 relates to the state vectors existing on either side of it. Thus, the following relations are written in a routine manner:

$$\begin{aligned} &\{Z\}_1^{\mathrm{L}} = [F]_1[P]_0\{Z\}_0^{\mathrm{L}}, \\ &\{Z\}_1^{\mathrm{R}} = [P]_1\{Z\}_1^{\mathrm{L}} = [P]_1[F]_1[P]_0\{Z\}_0^{\mathrm{L}} = [Q]_1[P]_0\{Z\}_0^{\mathrm{L}}, \\ &\quad\vdots \\ &\{Z\}_n^{\mathrm{R}} = [Q]_n[Q]_{n-1}\cdots[Q]_1[P]_0\{Z\}_0^{\mathrm{L}} = [S]\{Z\}_0^{\mathrm{L}}. \end{aligned} \tag{36}$$

It may be noted that the matrix $[S]$ is a 4×4 matrix:

$$[S] = \begin{bmatrix} S_{11} & S_{12} & S_{13} & S_{14} \\ S_{21} & S_{22} & S_{23} & S_{24} \\ S_{31} & S_{32} & S_{33} & S_{34} \\ S_{41} & S_{42} & S_{43} & S_{44} \end{bmatrix}. \tag{37}$$

Thus, depending upon the boundary conditions, the frequency equation will be obtained from equation (36).

3.1. BEAM CASES WITH LEFT END FREE

When the left end of the beam is free, one has $M = V = 0$ at station zero. Thus, equation (36) becomes

$$\begin{Bmatrix} -w \\ \psi \\ M \\ V \end{Bmatrix}_n^{\mathrm{R}} = [S] \begin{Bmatrix} -w \\ \psi \\ M = 0 \\ V = 0 \end{Bmatrix}_0^{\mathrm{L}} = \begin{bmatrix} S_{11} & S_{12} \\ S_{21} & S_{22} \\ S_{31} & S_{32} \\ S_{41} & S_{42} \end{bmatrix} \begin{Bmatrix} -w \\ \psi \end{Bmatrix}_0^{\mathrm{L}}. \tag{38}$$

3.1.1. *Free–free beam*

For a free–free beam, the right end of the beam is also free, having $M = V = 0$ at station n. Thus equation (38) becomes

$$\begin{Bmatrix} -w \\ \psi \\ 0 \\ 0 \end{Bmatrix}_n^{\mathrm{R}} = \begin{bmatrix} S_{11} & S_{12} \\ S_{21} & S_{22} \\ S_{31} & S_{32} \\ S_{41} & S_{42} \end{bmatrix} \begin{Bmatrix} -w \\ \psi \end{Bmatrix}_0^{\mathrm{L}}, \tag{39}$$

which leads to the frequency equation

$$\begin{vmatrix} S_{31} & S_{32} \\ S_{41} & S_{42} \end{vmatrix} = 0. \tag{40}$$

Since elements of $[S]$ are functions of ω^2, one can find the natural frequencies as those values of ω^2 that make the determinant, equation (40), zero.

3.1.2. *Other boundary conditions*

By extending the procedure discussed above, frequency equations can be derived for all the possible boundary conditions by noting that for a free end, $M = V = 0$; for a fixed end, $w = \psi = 0$; for a pinned end, $w = M = 0$; and for a sliding end, $\psi = V = 0$. The resulting frequency equations are as follows:

(i) free–free beam, $(S_{31}S_{42} - S_{41}S_{32}) = 0$;
(ii) free–fixed beam, $(S_{11}S_{22} - S_{21}S_{12}) = 0$;
(iii) free–pinned beam, $(S_{11}S_{32} - S_{31}S_{12}) = 0$;
(iv) free–sliding beam, $(S_{21}S_{42} - S_{41}S_{22}) = 0$;
(v) fixed–fixed beam, $(S_{13}S_{24} - S_{23}S_{14}) = 0$;
(vi) fixed–pinned beam, $(S_{13}S_{34} - S_{33}S_{14}) = 0$;
(vii) fixed–sliding beam, $(S_{23}S_{44} - S_{43}S_{24}) = 0$;
(viii) pinned–pinned beam, $(S_{12}S_{34} - S_{32}S_{14}) = 0$;

(ix) pinned–sliding beam, $(S_{22}S_{44} - S_{42}S_{24}) = 0$;
(x) sliding–sliding beam, $(S_{21}S_{43} - S_{41}S_{23}) = 0$. (41)

These are the unique combinations of the possible boundary conditions, and another set can be written with fixed–free, pinned–free, pinned–fixed, sliding–free, sliding–fixed and sliding–pinned boundaries which will lead to identical results as do their respective counterparts finally. Thus, all the 16 possible boundary conditions are addressed in the code developed.

3.2. MODE SHAPES

In order to determine the mode shapes, the general procedure adopted can be conceived from a discussion pertaining to the specific case of a free–free beam. Determination of the deformation modes for the free–free beam is discussed first, and the procedure for obtaining the rigid body modes for the unconstrained beam is addressed next. Thus, recalling equation (39), one has

$$S_{31}(-w)_0 + S_{32}(\psi)_0 = 0, \qquad S_{41}(-w_0) + S_{42}(\psi)_0 = 0. \tag{42}$$

From these equations, one can find ψ if the relative amplitude of $(-w)_0$ is assumed to be unity. Thus,

$$\psi_0 = -S_{31}/S_{32} = -S_{41}/S_{42}. \tag{43}$$

The relative amplitudes of $-w$, ψ, M and V can now be determined for each of the natural frequencies determined with the help of equation (36), written for any arbitrary station i as

$$\{Z\}_i^{\mathrm{R}} = [Q]_i[Q]_{i-1}\cdots[Q]_1[P]_0\{Z\}_0^{\mathrm{L}} = [Q]_i[Q]_{i-1}\cdots[Q]_1[R], \tag{44}$$

where

$$[R] = [P]_0\{1 \quad -S_{31}/S_{32} \quad 0 \quad 0\}^{\mathrm{T}}. \tag{45}$$

Since $[P]_0$, $[Q]_i$, $[Q]_{i-1}\cdots[Q]_1$ are known, one can determine the relative amplitudes of $\{Z\}_i^{\mathrm{R}} = \{-w \;\; \psi \;\; M \;\; V\}^{\mathrm{T}}$ for station i, and to the right of it from equations (44) and (45).

For a beam which is either unconstrained or partially constrained, rigid body modes occur with zero frequency. In the present transfer matrix procedure, since all stations can support springs, one can first determine a set of stations along the beam span at which placement of a set of springs would eliminate the unconstrained degrees of freedom. At such stations, linear and rotary springs of small stiffness are placed (K_w and K_ψ are chosen so that the stiffness of the spring supports is negligible compared to the beam stiffness, typically $K_w l^3/EI = K_\psi l/EI = 10^{-4}$). The code is run now in the usual manner, taking care to capture the rigid body modes, which will now occur at a frequency close to zero rather than at exactly zero frequency. The rigid body modes thus obtained will be found to be orthogonal to the deformation modes. This procedure will be illustrated in this paper subsequently through a numerical example.

3.3. ORTHOGONALITY RELATIONS AND GENERALIZED MASSES

The orthogonality relations for the beam with effects of shear, rotary inertia and sprung masses take the form

$$\sum_{i=0}^{n} [m_i w_{ij} w_{ik} + H_{11} J_i \psi_{ij} \psi_{ik}] + \sum_p m_p [w_{pj} + \xi_{pj}][w_{pk} + \xi_{pk}] = M_{jk}. \tag{46}$$

$M_{jk} = 0$ if $j \neq k$ is the orthogonality relation, and $M_{jk} = M_{jj}$ is the generalized mass when $j = k$, for any mode j. Furthermore, w_{ij} and ψ_{ij} are the values of the respective eigenvectors for the jth mode at station i. Finally, ξ_{pj} is the relative displacement of the sprung mass at station p relative to the beam deflected position in the jth mode, and the summation is made for all of the sprung masses. Finally, in equation (46), $H_{11} = -1$ when $H_1 = -1$, $H_{11} = 1$ when $H_1 = 1$ or -3, and $H_{11} = 0$ when $H_1 = 0$.

4. DETAILS OF THE COMPUTER CODE AND DEVELOPMENT OF SOME EXACT SOLUTIONS

By utilizing the analysis presented, a computer code has been developed in the FORTRAN language. The procedure adopted in the determination of the frequencies and validation of the results produced by the code are discussed in what follows.

4.1. PROGRAM DETAILS

The computer code developed can determine the natural frequencies, relative amplitudes of displacement, slope, bending moment and shear force, and performs checks on the orthogonality of normal modes. The generalized mass for each mode is also obtained in this process. The computer code is run on a WIPRO Super Genius 486 DX2 machine, with double precision arithmetic. The logic used in determining the frequencies is through a determinant search method. A small, initial value of the frequency is assumed as a guess, and the determinant for any chosen beam configuration (see equations (40) and (41)) is computed. The frequency is increased in small steps until the sign of the determinant is observed to change. Once a sign change is observed between two successive values of the assumed frequencies separated by a small increment, the determinant must have passed through a zero value somewhere in between these two assumed values of the frequency. Attempting to obtain the frequency which would produce an exact zero value of the determinant is not of practical interest. Thus, the criterion used for the determination of the natural frequency is either to check the difference between the positive and negative values of the successive determinants to be less than a prescribed accuracy measure (less than 10^{-30}), or to determine whether the frequency has converged to a pre-assigned number of significant figures (12–14 significant figures). If one of the above stated criteria cannot be achieved, the code chooses the other criterion for the termination of that particular frequency search. This frequency search is performed by halving the increment that existed when the sign of the determinant was originally sought, so that the subsequently obtained frequencies are separated by a halved interval, and this halving of the interval procedure continues until the convergence criterion is met.

Once the natural frequency to a desired accuracy is obtained, the relative amplitudes of displacement, slope, bending moment and shear force are obtained for each station, as discussed in section 3.2, the orthogonality checks are performed and the generalized masses are computed, as discussed in section 3.3.

4.2. EXACT SOLUTIONS

Exact solutions can be developed for certain cases of uniform beams. Some such solutions are obtained here for validating the results produced by the presently developed code. A pinned–sliding beam case is considered first. The boundary conditions for this case are

$$\eta = 0, \quad w = 0, \quad M = 0; \qquad \eta = 1, \quad V = 0, \quad \psi = 0. \tag{47}$$

By applying these boundary conditions in equations (17), one can show that $A_2 = A_4 = 0$ and

$$(P_1 + P_2) \cosh \lambda_1 \cos \lambda_2 = 0. \tag{48}$$

Thus,

$$\lambda_1 \neq 0 \quad \text{and} \quad \lambda_2 = (2N + 1)\pi/2, \qquad \text{where } N = 0, 1, 2, \ldots . \tag{49}$$

By substituting $\lambda = \pm \mathrm{i}(2N + 1)\pi/2$ in equation (13), one obtains a quadratic equation in ω^2, as

$$\omega^4 - C_1\omega^2 + C_2 = 0, \tag{50}$$

where

$$C_1 = KGA/(\rho I) + \pi^2(2N + 1)^2(E + KG)/(4\rho l^2),$$

$$C_2 = \pi^4(2N + 1)^4 EKG/(16\rho^2 l^4), \tag{51}$$

the solution of which is

$$\omega^2 = \{C_1 \pm \sqrt{[C_1^2 - 4C_2]}\}/2. \tag{52}$$

Solutions for ω are obtained for $N = 0, 1, \ldots$, and for positive and negative signs before the discriminant. These exact solutions are used for comparison of results produced by the transfer matrix code.

A similar procedure for the case of a sliding–sliding beam gives $\lambda = \pm \mathrm{i}\pi N$, $N = 0, 1, 2, \ldots$, which, introduced into equation (13), yields

$$C_1 = KGA/(\rho I) + \pi^2 N^2(E + KG)/(\rho l^2), \qquad C_2 = \pi^4 N^4 EKG/(\rho^2 l^4), \tag{53}$$

in equation (52), which is used for the determination of ω. Dolph [16] used a slightly different approach, and obtained an exact solution for the pinned–pinned beam. It may be noted that the exact solution for the pinned–pinned beam in [15] is identical to the sliding–sliding beam case obtained here.

Examination of equation (52) indicates that there are two families of frequencies, one for the negative sign before the discriminant and the other for the positive sign. One of these two families belongs to the interactions and resonances between the shear deformation and rotary inertia effects. These are the higher set of frequencies, obtained with a positive sign before the discriminant in equation (52) for any assigned value of N. The second set of frequencies belonging to the lower category are the counterparts for the classical Euler–Bernoulli theory eigenvalues, presently allowing for the shear and rotary inertia corrections. Frequencies corresponding to the higher set are identified as secondary modes, with an increasing order of numbering, in the discussion that follows.

5. RESULTS AND DISCUSSION

Several types of beam configurations with all possible boundary conditions, discontinuities in mass and stiffness distributions, variable axial tension or compression, and spring supports were solved by using the presently developed code. These results were compared with those available in the published literature [15–18], and excellent agreement was observed between the results compared. A typical set of results is presented in this

section to validate the present code. The examples are so chosen that each set of results presented below helps validate one key non-classical effect addressed by the present code.

5.1. EFFECTS OF SHEAR DEFORMATION AND ROTARY INERTIA

In order to validate the capability of the code in handling the shear deformation and rotary inertia effects, the following rectangular cross-section beam is taken: $L = 1$ m, $d/b = 0{\cdot}25$, $\bar{r}$ (least) $= 0{\cdot}025$, $G = 80$ GPa, $\rho = 7800$ kg/m^3, $K = 10(1 + \nu)/(12 + 11\nu)$, $E = 200$ GPa.

The beam is divided into 100 equal segments, and the mass and mass moment of inertia is lumped at the centroid of each segment. Thus, the discretized model has 101 stations. Segment 1, between station zero and station 1, has a length of $L/200$, as also does the last segment. The remaining segments have equal lengths, of $L/100$ each. The mass and mass moment of inertia lumped at station zero and those lumped at station 101 are zero, while the remaining stations have equal masses ($\rho AL/100$) and equal mass moments of inertia ($\rho IL/100$). All of the segments have the same flexural rigidity (EI) and shear stiffness (KGA). While addressing the flexural vibration in the flexible direction of the beam, I is taken as $bd^3/12$, while for vibration in the stiff direction, I is taken as $db^3/12$. By using this model, frequencies, mode shapes and generalized masses are obtained for a pinned–sliding beam and for a pinned–pinned beam. Exact solutions are also produced, as discussed in section 4.2. These results are tabulated in Tables 1–6.

5.1.1. *Pinned–sliding beam*

Results pertaining to the pinned–sliding beam from the exact solution for the Timoshenko beam theory are presented in the first four columns of Table 1. As discussed in section 4.2, two families of frequencies are obtained, one with a negative sign before the discriminant and the other with a positive sign before the discriminant. These exact frequencies are tabulated in an increasing order of magnitude, with the appropriate sign before the discriminant and the appropriate value of N that produced the frequency under reference also being noted against the frequency value.

The exact frequencies obtained in accordance with Euler–Bernoulli theory, and the presently computed frequencies by the code, are presented in the last two columns of the table.

The frequencies produced by the code, including the effects of shear deformation and rotary inertia, are presented in the fifth column of the table, and the type of the mode is identified from the mode shapes produced by the code.

An examination of these results indicates that an excellent agreement exists between the results produced by the present code and the corresponding exact solutions. The lowest ten modes of vibration in the flexible direction of the Timoshenko beam correspond to the lower family of eigenvalues of the exact solution, and correspond to the lowest ten frequencies produced by Euler–Bernoulli theory, the difference between the two sets being the inclusion of shear and rotary inertia effects in the former set and their suppression in the latter set.

An examination of the frequencies pertaining to the vibration of the beam in the stiffer direction reveals the fifth, seventh and the ninth modes in the increasing order of frequency correspond to the higher family of eigenvalues in the exact solution for the Timoshenko beam. These modes are identified as secondary modes in the table referred to, and their mode shapes resemble the first, second and third mode shapes of the lower family frequencies. These mode shapes are presented in Figure 3. However, their occurrence is somewhere in between the higher modes of the lower family of the eigenvalues.

TABLE 1

Frequencies for a pinned–sliding beam (rad/s)

	Results from Timoshenko beam theory					Results from Euler–Bernoulli beam theory	
	Exact solutions			Solutions from transfer matrix method			
Sl. no.	Value of N	Sign	Frequency	Frequency	Mode type	Exact frequency	Computed frequency
Modes in flexible direction ($\bar{r} = 0{\cdot}025$)							
1	0	–	311·41	311·41	Mode 1	312·354	312·354
2	1	–	2 737·86	2 737·86	Mode 2	2 811·188	2 811·188
3	2	–	7 286·65	7 286·47	Mode 3	7 808·857	7 808·857
4	3	–	13 499·80	13 498·70	Mode 4	15 305·360	15 305·358
5	4	–	20 925·30	20 921·06	Mode 5	25 300·696	25 300·689
6	5	–	29 196·20	29 184·20	Mode 6	37 794·867	37 794·844
7	6	–	38 043·10	38 018·20	Mode 7	52 787·873	52 787·809
8	7	–	47 276·90	47 229·22	Mode 8	70 279·712	70 279·561
9	8	–	56 767·10	56 684·75	Mode 9	90 270·386	90 270·043
10	9	–	66 424·50	66 292·48	Mode 10	112 759·890	112 758·763
Mode in stiff direction ($\bar{r} = 0{\cdot}1$)							
1	0	–	1 193·54	1 193·54	Mode 1	1 249·417	1 249·417
2	1	–	8 390·28	8 390·00	Mode 2	11 244·754	11 244·754
3	2	–	17 823·90	17 821·40	Mode 3	31 235·428	31 235·427
4	3	–	27 672·10	27 662·48	Mode 4	61 221·438	61 221·432
5	0	+	30 862·20	30 857·23	Secondary mode I	—	—
6	4	–	37 522·00	37 497·81	Mode 5	101 202·790	101·202·758
7	1	+	39 512·10	39 500·49	Secondary mode II	—	—
8	5	–	47 289·60	47 240·74	Mode 6	151 179·470	151 179·376
9	2	+	51 665·50	51 639·00	Secondary mode III	—	—
10	6	–	56 970·10	56 884·02	Mode 7	211 151·490	211 151·235

Furthermore, the orthogonality checks and generalized masses for the modes in the stiff direction are presented in Table 2, and the normalization factors (the maximum amplitude of the displacement in any given mode shape) in Table 3. These results show that the orthogonality relations are satisfied even between the primary and the secondary modes,

TABLE 2

Orthogonality checks and generalized masses for a pinned–sliding beam (*modes are not normalized*): *modes in stiff direction*

	M_{ij}					
Mode j	Mode $i = 1$	Mode $i = 2$	Mode $i = 3$	Mode $i = 4$	Mode $i = 5$	Mode $i = 6$
1	55·5761	−0·3526E − 10	−0·2419E − 10	0·6863E − 11	0·3323E − 11	−0·9585E − 12
2		14·227	−0·1523E − 11	0·2558E − 11	−0·1661E − 10	−0·3654E − 11
3		Symmetric	12·604	0·6034E − 11	−0·1724E − 11	−0·1506E − 11
4				14·342	0·5633E − 11	−0·3589E − 11
5					11·963	0·3424E − 11
6						17·258

TABLE 3

The maximum displacement amplitude in the mode shape (normalization factor, NF): modes in the stiff direction

Mode no.	*NF*	Mode no.	*NF*
1	0·68195	7	0·0299574
2	0·334052	8	0·419933
3	0·312456	9	0·0320118
4	0·335506	10	0·470567
5	0·014671	11	0·298769
6	0·673879	12	0·523872

revealing that the secondary modes are indeed part of the complete solution for the Timoshenko beam theory. However, when a comparison is to be made with the Euler–Bernoulli theory results, the lower family of eigenvalues are to be used to establish the influence of shear and rotary inertia effects. The higher family of eigenvalues are a consequence of interaction between the shear and rotary inertia effects themselves, as noted in reference [16].

TABLE 4

Frequencies for a pinned–pinned or sliding–sliding beam (rad/s)

	Results from Timoshenko beam theory					Results from Euler–Bernoulli beam theory	
	Exact solutions			Solutions from transfer matrix method			
Sl. no.	Value of N	Sign	Frequency	Frequency	Mode type	Exact frequency	Computed frequency
Modes in flexible direction ($\bar{r} = 0{\cdot}025$)							
1	1	–	1 234·53	1 234·53	Mode 1	1 249·417	1 249·417
2	2	–	4 774·16	4 774·11	Mode 2	4 997·668	4 997·668
3	3	–	10 215·00	10 214·46	Mode 3	11 244·754	11 244·753
4	4	–	17 086·30	17 084·01	Mode 4	19 990·674	19 990·670
5	5	–	24 974·00	24 966·91	Mode 5	31 235·428	31 235·414
6	6	–	33 561·10	33 543·95	Mode 6	44 979·016	44 978·976
7	7	–	42 620·90	42 585·97	Mode 7	61 221·438	61 221·338
8	8	–	51 996·30	51 932·98	Mode 8	79 962·695	79 962·490
9	9	–	61 579·30	61 474·14	Mode 9	101 202·790	101 202·437
10	10	–	71 295·80	71 132·51	Mode 10	124 941·710	124 942·368
Modes in stiff direction ($\bar{r} = 0{\cdot}1$)							
1	1	–	4 271·58	4 271·54	Mode 1	4 997·668	4 997·668
2	2	–	12 999·10	12 998·09	Mode 2	19 990·674	19 990·674
3	3	–	22 735·40	22 730·06	Mode 3	44 979·016	44 979·014
4	1	+	29 482·00	29 477·82	Shear mode*	—	—
5	4	–	32 605·30	32 589·49	Mode 4	79 962·695	79 962·681
6	2	+	34 493·40	34 485·96	Secondary mode I	—	—
7	5	–	42 417·20	42 382·05	Mode 5	124 941·710	124 941·658
8	3	+	45 338·90	45 321·07	Secondary mode II	—	—
9	6	–	52 140·10	52 074·31	Mode 6	179 916·060	179 915·905
10	4	+	58 326·30	58 288·52	Secondary mode III	—	—

*$\sqrt{KGA/\rho I} = 29481.98$

TABLE 5

Orthogonality checks and generalized masses for pinned–pinned beam (modes not normalized): modes in stiff direction

	M_{ij}					
Mode j	Mode $i=1$	Mode $i=2$	Mode $i=3$	Mode $i=4$	Mode $i=5$	Mode $i=6$
1	20·2959	−0·1623E − 10	−0·6646E − 11	−0·4226E − 11	0·3973E − 11	0·3550E − 11
2		12·6788	−0·1124E − 11	−0·1269E − 10	0·1376E − 10	0·8727E − 11
3		Symmetric	13·2445	0·2061E − 11	−0·5064E − 11	−0·8194E − 11
4				2·34198	0·1777E − 11	−0·1563E − 11
5					15·7865	0·2678E − 11
6						1·24302

5.1.2. *Pinned–pinned beam*

Results pertaining to the pinned–pinned beam for the numerical example given in section 5.1.1 are presented in Tables 4–6. The agreement between the exact solutions and the results produced by the present code is excellent.

The frequencies for the beam vibration in the stiff direction show certain interesting features. In particular, the mode at serial number 4, when examined carefully, shows almost negligible relative displacement (see Table 6), an order of magnitude smaller generalized mass in comparison to the other modes, and a constant value of shearing force (relative amplitude = $0{\cdot}20341856 \times 10^{10}$ N) along the entire beam span. Furthermore, the frequency of this mode is found to be equal to the value of $\sqrt{KGA/\rho I}$. The bending slope for this mode is seen to be 1·0004238 all along the span, except at its ends, where it is 1·0. This mode is thus identified as the shear mode in Table 4. Furthermore, the modes at serial numbers 6, 8 and 10 are identified as secondary modes I, II and III respectively, and these modes belong to the family of exact solutions with a positive sign before the discriminant. The generalized masses for these modes are an order of magnitude smaller than the remaining ones shown in Table 5, obey the orthogonality relations, and have a relatively smaller mode shape amplitude (see Table 6). The mode shapes of secondary modes I, II and III are similar to the corresponding primary modes, modes 1, 2 and 3 respectively, and are of opposite phase (similar to the trends shown in Figure 3).

Finally, another set of results was produced with $E/KG = 3{\cdot}2$ and for various values of $\bar{r}$. The primary modes were identified, compared with the corresponding classical

TABLE 6

The maximum displacement amplitude in the mode shape (normalization factor, NF): modes in the stiff direction

Mode no.	*NF*	Mode no.	*NF*
1	0·404263	7	0·394985
2	0·313476	8	0·0319035
3	0·321201	9	0·444589
4	0·126654E − 10	10	0·0311850
5	0·353436	11	0·497048
6	0·0247448	12	0·550903

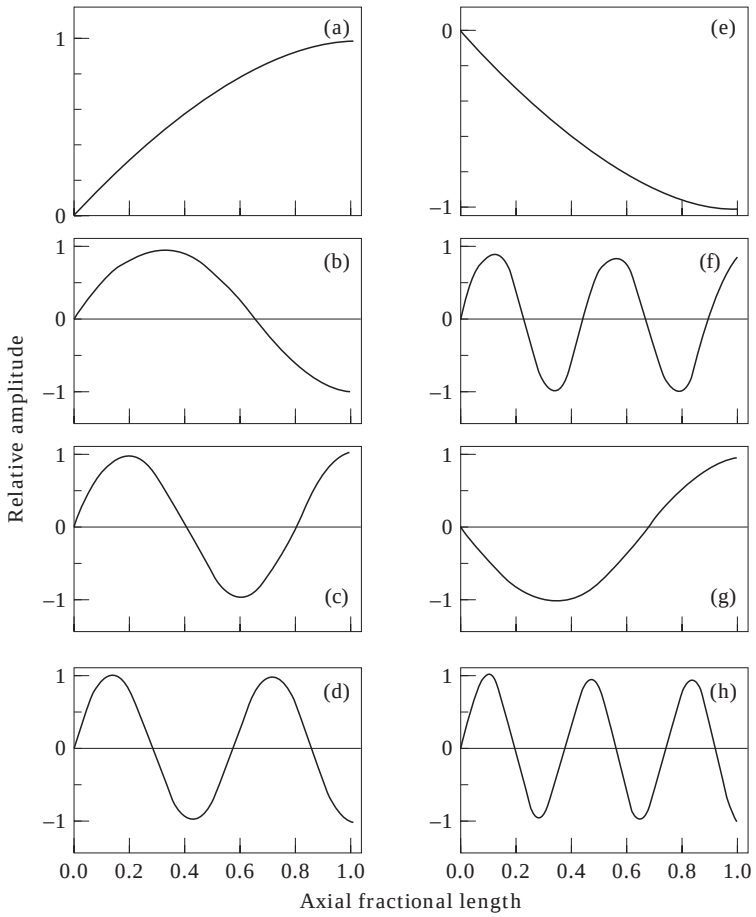

Figure 3. The mode shapes of pinned–sliding beam.

Euler–Bernoulli frequencies, and their ratios were compared to those presented in reference [19]. Good agreement is found here.

It may be noted that the exact solutions for frequencies of pinned–pinned beam are identical to those for sliding–sliding beam. It was verified that the results produced by the code for the sliding–sliding beam are almost identical to those of the pinned–pinned beam. Thus, the results presented in Table 4 are also applicable to the sliding–sliding beam case. However, the mode shapes are different and, for brevity, are not presented here.

5.2. EFFECTS OF VARIABLE AXIAL TENSION AND SPRING SUPPORTS

In order to validate the code for beam cases with variable axial tension, the beam example given in section 5.1 is assumed to rotate about an axis passing through its built-in end, the plane of rotation of the beam being perpendicular to the axis of rotation in one case (radial rotating beam), and the beam being lifted out of the plane of rotation by an angle β_{pc} in another case (preconed beam).

For a preconed beam with a precone β_{pc}, each mass m_i of the discretized beam model is subjected to a centrifugal force $m_i\Omega^2 r_i \cos^2 \beta_{pc}$, since the rotation vector now has to be resolved for the blade orientation. Associated with this, the beam has a softening effect

$m_i\Omega^2 \sin^2 \beta_{pc}$ in its flapping direction (out-of-plane motion). In the in-plane (lead–lag) direction, however, the softening effect is $-m_i\Omega^2$.

Thus, in the transfer matrix code, one has to provide the details of the tension in each segment as well as the softening effect due to rotation. For any segment i bounded between stations $i-1$ and i, the tensile force is computed from the following scheme:

$$P_n = (\Omega^2 \cos^2 \beta_{pc}) m_n R, \qquad P_{n-1} = P_n + (\Omega^2 \cos^2 \beta_{pc}) m_{n-1}(R - l_n), \qquad \ldots,$$

$$P_i = P_{i+1} + (\Omega^2 \cos^2 \beta_{pc}) m_i \left\{ R - \sum_{k=i+1}^{n} l_k \right\}. \tag{54}$$

Here, P_i is the tension in the ith segment of the beam, R is the radius of the beam ($R = L$), m_i is the mass lumped at the ith station, and l_k is the length of the kth segment.

The softening effect for flapping motion is provided by springs with negative stiffness, $K_{wi} = -m_i\Omega^2 \sin^2 \beta_{pc}$, $i = 0, 1, \ldots, n$. While solving for the in-plane vibrations, the lead–lag softening is simulated in a similar manner, with a negative spring stiffness of $-m_i\Omega^2$, $i = 0, 1, 2, \ldots, n$.

The results thus produced for a radial rotating beam with $\beta_{pc} = 0$, and rotating with an angular velocity $\Omega = \omega_1 = 3{\cdot}51602\sqrt{EI/\rho AL^4}$, are presented in Table 7. A comparison of these results with those published in reference [10] shows excellent agreement for the Euler–Bernoulli beam theory cases. The effects of shear and rotary inertia are seen to be more pronounced for the stiff in-plane modes, as expected, and also on higher modes for the out-of-plane vibration.

Next, a beam case representative of an advanced turboprop blade is addressed. This beam has a thickness ratio of 0·05, precone of 15°, and is subjected to speeds of up to $\Omega/\omega_1 = 1{\cdot}0$. The beam model discussed earlier is solved by using the present code, and the results obtained are presented in Table 8, where they are compared with linear and non-linear beam theory results, including the Coriolis effects of reference [6], and the MSC/NASTRAN calculations of reference [6]. The results produced by the present theory are in excellent agreement with those of reference [6], since the Coriolis effects and geometric non-linear effects are negligible for thin blades with precones of up to 15°. Furthermore, the effects of shear and rotary inertia are negligible for thin blades vibrating in their flexible direction, and these effects will become significant for the modes in the stiff direction.

These examples validate the capability of the present code in handling variable axial tension and spring supports.

TABLE 7

The effect of rotation upon the frequency ratios, ω/λ_1, of a cantilever blade: $d/b = 0{\cdot}25$

Ω/ω_1	Mode no.	Shear deformation (SD) and rotary inertia (RI) effects neglected		SD and RI effects included: present	Mode type
		[10]	Present		
1·0	1	5·1916	5·1914	5·1462	Flap mode
	2	14·1480	14·1480	12·9580	Lead–lag mode
	3	23·7830	23·7825	22·8819	Flap mode
	4	63·4570	63·4610	58·2308	Flap mode
	5	88·5200	88·5277	58·8228	Lead–lag mode

TABLE 8

Frequency ratios, ω/λ_1, for a preconed, rotating cantilever blade: $\beta_{pc} = 15^\circ$, $d/b = 0{\cdot}05$

Ω/ω_1	Mode no.	Beam theory results [6] (Coriolis effects included)			Present results excluding Coriolis effects
		Linear	Non-linear	MSC/NASTRAN	
0·3	1	3·6776	3·6804	3·7062	3·6777
	2	22·1849	22·1860	22·2934	22·1866
	3	61·8467	61·8475	62·1044	61·8547
0·5	1	3·9476	3·9652	3·9950	3·9481
	2	22·4498	22·4572	22·5585	22·4516
	3	62·1113	62·1169	62·3354	62·1195
0·8	1	4·5356	4·6094	4·6451	4·5367
	2	23·0828	23·1182	23·2026	23·0847
	3	62·7514	62·7763	62·8837	62·7595
1·0	1	5·0138	5·1444	5·1781	5·0157
	2	23·6522	23·7203	23·7926	23·6541
	3	63·3360	63·3821	63·4078	63·3441

5.3. VARIABLE AXIAL COMPRESSION: CASES OF BEAM BUCKLING

If a beam has axial loads at both ends, and the load variation is such that a tensile load P_1 applied at one end varies as $P_1 - Wx$, with the load at the other end, $x = L$, being $P_1 - WL$, then the beam might be subjected to variable axial tension in a certain portion of the beam span, with a variable axial compression in its remaining portion depending upon W. The fundamental frequency parameter ω_1/λ_1 for such a beam is plotted against WL^3/EI for various cases of P_1/WL for the case of pinned–pinned beams in Figure 4(a), and for fixed–fixed beams in Figure 4(b). Here, ω_1 is the fundamental natural radian frequency, and $\lambda_1 = \sqrt{EI/\rho AL^4}$. These results are compared to those available in reference [20], and excellent agreement is found for the buckling boundaries and the frequency parameter variations in all the cases considered.

5.4. BEAMS WITH VARIABLE MASS AND STIFFNESS DISTRIBUTION

In order to validate the present code for cases of beams with variable mass and stiffness distributions, several cases of tapered cantilever beams are solved. These beams have a square cross-section ($b_0 = d_0$) at the root, and the breadth and depth at any section distant x from the root are defined by

$$b = b_0(1 - \beta\eta), \qquad d = d_0(1 - \delta\eta), \qquad \eta = x/L. \tag{55}$$

For these beams, the following characteristics are assumed: $L = 1$ m, $b_0 = d_0 = \bar{r}L\sqrt{(12)}$, $E = 200$ GPa, $G = 80$ GPa, $E/KG = 3$. The discretization procedure of the beam involves computation of the segmental masses, lumping them at the centroid of the segment, numbering the stations from the left end (free end, station 0) to the right end (built-in end, station n, $n = 101$ for 100 segments) with all the intermediate mass points having numbers $1, 2, \ldots, n - 1$; and computing the flexural rigidity and shear stiffness of each segment as applicable at its mid-span location. With the beam mass, and mass moment of inertia lumped at 100 stations, frequencies were determined for various cases of β and δ, by using Euler–Bernoulli theory and Timoshenko theory. The frequency ratio, the square of the

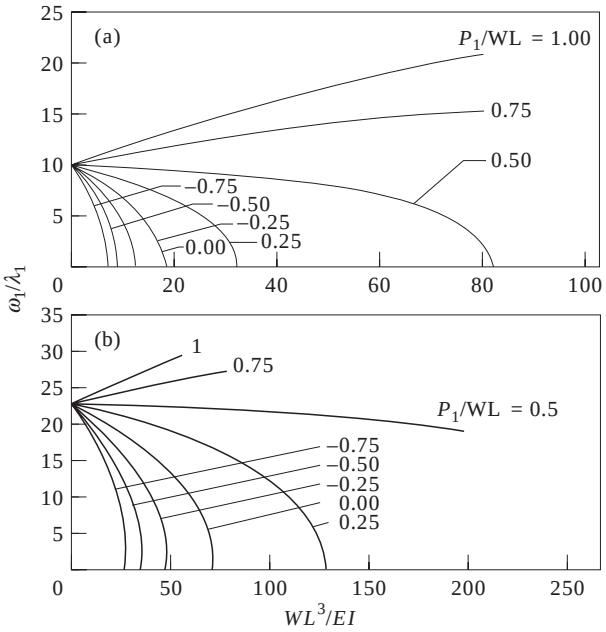

Figure 4. The effect of linearly varying axial loads on the fundamental frequency: (a) pinned–pinned beam; (b) fixed–fixed beam.

frequency including shear and rotary inertia effects (p_t^2) to the square of the frequency neglecting shear and rotary inertia effects (p_c^2), is calculated for the first five modes, and for various values of the non-dimensional radius of gyration of the beam at the root section. These results are plotted in Figure 5 for the case of $\beta = 0$, $\delta = -0{\cdot}5$. Another set of results for the case $\beta = \delta = -0{\cdot}5$ is also shown for $\bar{r} = 0{\cdot}08$. These results are compared with those presented by Carnegie and Thomas [8], and excellent agreement is found. This example illustrates the capability of the code in handling variable mass and stiffness characteristics of beams.

5.5. TREATMENT OF UNCONSTRAINED BEAMS: DETERMINATION OF RIGID BODY MODES AND DEFORMATION MODES

For beams which are unconstrained or only partially constrained against rigid body displacements by their external support system, the vibration frequencies corresponding

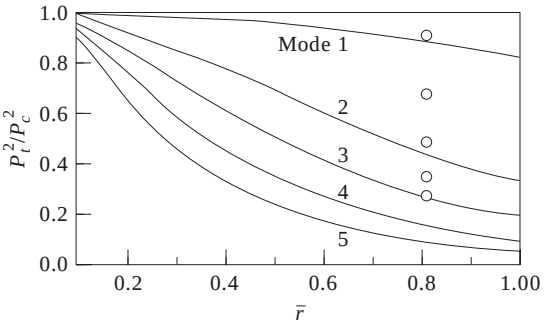

Figure 5. Frequency parameter variation for tapered Timoshenko beams. ——, $\beta=0$, $\delta = -0{\cdot}5$; ○, $\beta = \delta = -0{\cdot}5$.

TABLE 9

Rigid body mode and deformation mode frequencies (rad/s), *and generalized masses*, *for a free–free beam*: *spring stiffness for stations* 0, 50, 51 *and* 101 $= K_w L^3/EI = K_\psi L/EI = 0{\cdot}0001$

Mode no.	Exact solution	Solution without any spring supports		Solution including spring supports	
		Euler–Bernoulli	Timoshenko	Euler–Bernoulli	Timoshenko
Rigid body modes					
I	0	—	—	3·56	3·56
II	0	—	—	15·61	15·55
Deformation modes					
1	2 832·29	2 832·73	2 760·53	2 832·98	2 760·77
2	7 807·31	7 809·36	7 284·11	7 809·62	7 284·34
3	15 305·45	15 311·06	13 498·00	15 311·32	13 498·22
4	25 300·69	25 312·61	20 916·13	25 312·87	20 916·33
5	37 794·87	37 816·63	29 169·62	37 816·88	29 169·81
6	52 787·87	52 823·77	37 981·16	52 824·02	37 981·34

Generalized masses for Timoshenko beam

	Rigid body modes		Deformation modes			
	I	II	1	2	3	4
Generalized mass	381·74	69·55	60·76	64·69	69·90	76·15

to the rigid body motions are zero. Determination of the rigid body modes and the corresponding generalized masses can be accomplished in the present transfer matrix method by adding small spring constraints to the unrestrained degrees of freedom [21]. This procedure is illustrated for the case of the beam example given in section 5.1, with free–free boundary conditions.

The discretized beam model, developed as discussed earlier, is solved for free–free boundary conditions, and the natural frequencies and mode shapes for the case of deformation modes are determined, including or excluding the effects of shear deformation and rotary inertia. Next, springs are provided at four stations; namely, at the two extreme ends of the beam and at the two central stations (stations zero, 50, 51 and 101) with stiffnesses $K_w L^3/EI = K_\psi L/EI = 0{\cdot}0001$. These springs are sufficient to constrain the rigid body degrees of freedom. The code is run again for the determination of the frequencies, mode shapes and generalized masses as before. This model provides two rigid body modes along with the deformation modes. The results thus obtained, along with exact solutions, are shown in Table 9, and the mode shapes are shown in Figure 6.

A comparison of these results indicates that the rigid body modes obtained presently are 3·55 rad/s and 15·55 rad/s, respectively, rather than an exact zero for each of these rigid body modes. However, in comparison to the deformation modes, the present rigid body mode frequencies may be regarded as zero. Furthermore, the deformation modes are essentially the same whether or not the spring supports are placed. Finally, the orthogonality relations are found to be satisfied, and the generalized masses of the deformation modes remain essentially unchanged whether or not the spring constraints are

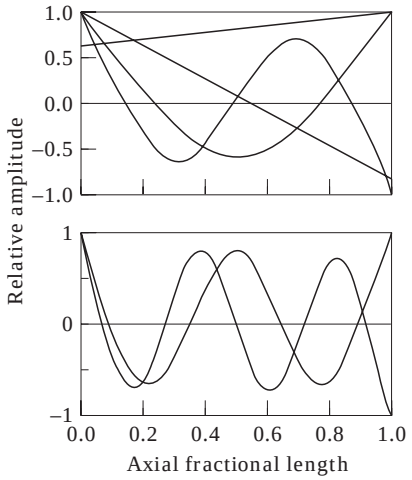

Figure 6. Rigid body modes and deformation modes of a free–free Timoshenko beam.

included in the beam model. Thus, the presently developed transfer matrix procedure can effectively handle unconstrained or partially constrained beams.

6. CONCLUSIONS

The transfer matrix method presented in this paper has been shown to produce accurate solutions with all possible boundary conditions, and with complicating effects such as shear deformation, rotary inertia, discontinuities in mass and stiffness distributions, and spring supports. The method is quite simple, and does not require a large space while the program is run on the computer. The method, in its present form, has not introduced any convergence problems or computational difficulties.

In view of the simplicity in the analysis, the lower space requirement on the computer, and the excellent accuracy of the results produced by the method, it is believed that the presently developed computer code would be of considerable use to the designer.

ACKNOWLEDGMENTS

This research effort is supported by the Indian Space Research Organisation, Vikram Sarabhai Space Centre, Trivandrum. The financial support rendered by ISRO is gratefully acknowledged. The authors express their sincere appreciation to Dr I. Gopal Reddy, Director, NBKRIST, Vidyanagar; to Professor J. S. Rao, IIT, Delhi; and to Dr A. R. Acharya, Dr G. V. Rao and Mr M. N. G. Elayathu of VSSC, Trivandrum for their encouragement and support.

REFERENCES

1. C. L. Dym and I. H. Shames 1973 *Solid Mechanics*: *A Variational Approach*. New York: McGraw-Hill.
2. K. B. Subrahmanyam 1993 *Journal of Reinforced Plastics and Composites* **12**, 642–669. Analysis of thin-walled composite beams by energy method.
3. J. S. Rao, S. V. Kulkarni and K. B. Subrahmanyam 1981 *Transactions of the American Society of Mechanical Engineers*, *Journal of Applied Mechanics* **48**, 672–673. Application of the Reissner method to a Timoshenko beam.

4. K. B. Subrahmanyam, S. V. Kulkarni and P. M. Rao 1982 *Journal of Sound and Vibration* **81**, 141–146. Dean and Plass method calculation of flexural frequencies of Timoshenko beams.
5. H. Leipholz 1976 *Shock and Vibration Digest* **8**, 3–18. Use of Galerkin's method for vibration problems.
6. K. B. Subrahmanyam and K. R. V. Kaza 1987 *International Journal of Mechanical Science* **29**, 29–43. Nonlinear flap–lag–extensional vibration of rotating, pretwisted, preconed beams including Coriolis effects.
7. M. G. Salvadori 1949 *Transactions of the American Society of Civil Engineers* **2441**, 590–636. Numerical computation of buckling loads by finite differences.
8. W. Carnegie and J. Thomas 1972 *Transactions of the American Society of Mechanical Engineers*, *Journal of Engineering for Industry* **94**, 267–278. The effect of shear deformation and rotary inertia on the lateral frequencies of cantilever beams in bending.
9. K. B. Subrahmanyam and A. W. Leissa 1985 *Journal of Sound and Vibration* **98**, 1–11. An improved finite difference analysis of uncoupled vibrations of cantilever beams.
10. K. B. Subrahmanyam and K. R. V. Kaza 1986 *Transactions of the American Society of Mechanical Engineers*, *Journal of Vibration*, *Acoustics*, *Stress and Reliability in Design* **108**, 140–149. Vibration and buckling of rotating, pretwisted, preconed beams including Coriolis effects.
11. H. Holzer 1921 *Die Berechnung der Drehschwingungen*. Berlin: Springer-Verlag.
12. N. O. Myklestad 1944 *Journal of Aeronautical Sciences*, 153–162. A new method of calculating natural modes of uncoupled bending vibrations.
13. T. J. McDaniel and J. P. Henderson 1974 *Shock and Vibration Digest* **6**(1), 13–19; **6**(2), 3–18. A review of transfer matrix vibration analysis of skin–stringer structures—Parts I and II.
14. E. C. Pestel and F. A. Leckie 1963 *Matrix Methods in Elastomechanics*. New York: McGraw-Hill.
15. W. D. Pilkey and P. Y. Chang 1978 *Modern Formulas for Statics and Dynamics*. New York: McGraw-Hill.
16. C. L. Dolph 1954 *Quarterly Journal of Applied Mechanics* **12**, 175–180. On the Timoshenko theory of transverse beam vibrations.
17. R. D. Blevins 1973 *Formulas for Natural Frequency and Mode Shape*. New York: Van Nostrand Reinhold.
18. D. J. Gorman 1975 *Free Vibration Analysis of Beams and Shafts*. New York: John Wiley.
19. J. G. Sutherland and L. E. Goodman 1951 *Report No. N6-ORI-71*, *Task order VI*, *Project NR-064-183*, *University of Illinois*. Vibrations of prismatic bars including rotary inertia and shear.
20. W. M. Laird and G. Fauconneau 1966 *NASA Report NASA-CR-653*, *University of Pittsburg*. Upper and lower bounds for eigenvalues of vibrating beams with linearly varying axial load.
21. R. W. Clough and J. Penzien 1993 *Dynamics of Structures*. New York: McGraw-Hill.

APPENDIX A: NOMENCLATURE

A	cross-sectional area
A_1, A_2, A_3, A_4	arbitrary constants
b, d	breadth and thickness of beam
$[B]$	matrix, see equation (17)
C_1, C_2	coefficients, see equation (52)
E, G	Young's modulus and shear modulus, respectively
$[F], [P]$	field and point transfer matrices, respectively
H_1, H_2, H_{11}	coefficients used to invoke or suppress shear and rotary inertia effects
i, j, k, p	dummy indices
I	second moment of area
J	mass moment of inertia
K	shear coefficient
K_{12}, K_2	stiffness of springs used for sprung mass
K_w, K_ψ	linear and rotational spring stiffnesses
l_i	length of segment i
L	span of beam
m_i	mass lumped at the ith station
m_k	sprung mass

M, V	bending moment and shear force, respectively
M_{ij}	generalized mass if $i = j$, equal to 0 if $i \neq j$
n	number of stations
N	integer in Timoshenko beam exact solution
P	axial force
$\bar{r}$	$=\sqrt{I/AL^2}$, non-dimensional radius of gyration
w	displacememt
x	axial co-ordinate
$\{Z\}$	state vector, see equation (18)
$\beta, \gamma, \tau, \sigma$	see equation (11)
β, δ	taper parameters, see equation (55)
β_{pc}	blade precone angle
η	$=x/L$, axial fractional length
λ_1, λ_2	roots, see equation (14)
$\Lambda, \Lambda_1, \Lambda_2$	see equation (21)
μ	$=\rho A$, mass per unit length
ν	Poisson ratio
ρ	mass density
ω	natural radian frequency
Ω	rotational speed of beam
ψ	bending slope in Timoshenko beam theory, and total slope in Euler–Bernoulli theory
ζ	see equation (6)